Photocatalytic Self Cleaning Textile Fibers by Coaxial Electrospinning

N. M. Bedford[†,§] and A. J. Steckl*,[†,‡]

Nanoelectronics Laboratory, Department of Electrical and Computer Engineering, and Department of Chemical and Materials Engineering, University of Cincinnati, Cincinnati, Ohio 45221

ABSTRACT Photocatalytic self-cleaning textile fibers have been created using coaxial electrospinning. This is accomplished by electrospinning cellulose acetate as the core phase and a dispersion of nanocrystalline TiO_2, a well-known photocatalyst, in the sheath phase. A simple deacetylation step after the initial electrospinning yields self-cleaning textile fibers. Self-cleaning activity is exhibited at moderate power densities in indoor lighting conditions. Nanofibers created from coaxial electrospinning outperform TiO_2 surface-loaded nanofibers obtained by conventional electrospinning. Surface-loaded fibers degrade blue dye stains only to a minimum of 20 % of the initial concentration, whereas fibers created by coaxial electrospinning fully degrade stains (in 7−8 h).

KEYWORDS: coaxial electrospinning • textile fibers • photocatalysis • self-cleaning • TiO_2

INTRODUCTION

Chemical degradation and self-cleaning by hydrophilic semiconductor photocatalysts, such as titania (TiO_2), have a wide range of applications including toxic chemical decomposition (1−3), protective/self-cleaning clothing (4),self-cleaning glass (5), and self-cleaning membranes (6). Photocatalytic activity is initiated when incident photons are absorbed by the photocatalyst creating excited electrons in the conduction band and holes in the valence band (7). These electrons and holes lead to the formation of hydroxyl and oxygen radicals, which react with chemicals at the surface of the photocatalyst. Of particular note, chemically protective and self-cleaning clothing have obvious health, environmental, and military applications. Studies have been performed on titania treated textile materials, such as natural cotton (4, 8), chemically modified cotton (9), polyamide fibers (10), and chemically modified wool-like fibers (11). The chemical modification performed increases the number of hydroxyl or carboxylic acid groups on the surface of the fiber, which have shown to adhere very well to titania (9, 10). In these studies, the radiation used was often chosen to mimic the sun's spectrum at relatively high power densities. Typically, the UV component of the solar spectrum (200−400 nm) is responsible for photocatalytic activity. Somewhat surprisingly, photocatalytic self-cleaning is rarely tested in light of longer wavelengths and lower intensities resembling typical indoor working conditions.

A major shortcoming of these treated textiles is the poor surface-to-volume ratio (SVR), limiting the overall photocatalytic activity. Electrospinning (12) has become an extremely versatile technique for the formation of fibers of various materials with applications including (but not limited to) tissue engineering (13), drug delivery (14), sensors (15), and superhydrophobicity (16, 17). To increase the SVR, electrospinning has been previously implemented to create non-woven fibrous TiO_2-based meshes by the electrospinning of a titania precursor followed by calcination (18) or using plasma treatment of electrospun fibers followed by repeated cycles of surface attachment of TiO_2 nanoparticles on the surface (19). In these previous electrospinning reports, the materials electrospun were not based on typical materials used for clothing/textile applications.

In this study, photocatalytic self-cleaning textile fibers with high SVR are created using the coaxial electrospinning method (20−23). Cellulose acetate (CA) is used as the core phase which after a deacetylation step becomes cellulose. Cellulose, a biopolymer of consisting of β-1,4-glycosidic-linked D-glucose units, is one of the most abundant naturally occurring materials and is commonly found in green plant cell walls and wood (24). Cotton and cotton textiles contain as much as 90 % cellulose. A dispersion of TiO_2 nanoparticles (here the Degussa P-25 mixture of titania phases) with and without a low concentration of CA is used as the sheath phase to disperse titania nanoparticles along the fibers' outer surface. The titania nanoparticles attach to the electrospun fiber in flight by adhesion to hydroxyl groups already present in the CA. A simple deacetylation step produces cellulose fibers. The coaxial electrospun fibers show self-cleaning effects in indoor lighting conditions and outperform electrospun cellulose fibers surface loaded with TiO_2. While the vast majority of the light used in these experiments is above the considered cutoff wavelength of titania (~400 nm), photocatalytic activity is still observed due to titania's superior properties in charge-pair recombination lifetime, interfacial charge transfer rate, and near band gap light absorption (7). In particular, mixed anatase/rutile phase titania (such as P-25) promotes stable charge separation because
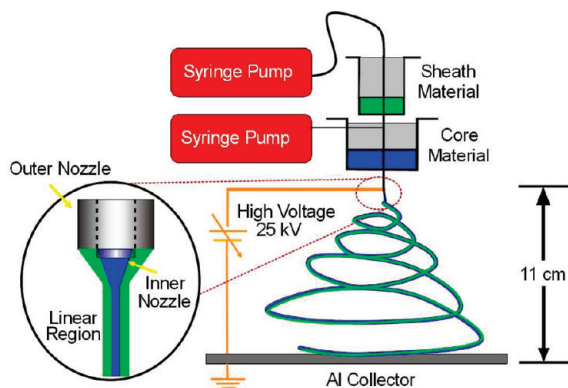
FIGURE 1. Schematic of coaxial electrospinning setup. The inset shows an illustration of a coaxial jet under applied voltage.

of unique charge trapping sites found between the two phases (25, 26). It has been shown that TiO_2 can photocatalytically outperform materials with smaller band gaps at these wavelengths because of these superior properties (27). Furthermore, exposure to acidic environments (28, 29) and number of peripheral hydroxyl groups (30) have shown to increase photocatalytic activity. The photocatalytic fibers maintain their self-cleaning properties after multiple staining and washing steps.

EXPERIMENTAL SECTION

Materials. CA (39.8% acetyl content, M_w = 30 000) was purchased from Sigma-Aldrich. Titania nanoparticle powder (Degussa Aeroxide P-25, mixed anatase/rutile phase, average diameter of 21 nm) was purchased from Acros Organics. Keyacid Blue FG (Keystone Aniline Corporation), Sulforhodamine 640 (Exciton) and red wine were used as staining agents. All other chemicals were purchased from industrial sources used without any further purification.

Sample Preparation. Electrospinning solutions of CA were made to a concentration of 17 wt % in 80/20 acetic acid/water (31). CA was added to the acetic acid solution and sonicated at low power until all the CA dissolved. For coaxial electrospinning, sheath solutions of TiO_2/CA were made at concentrations of 4 wt % TiO_2 and 2 wt % CA in 60/25/15 acetic acid/acetone/water by volume. The titania was added to a solution of acetic acid and water, sonicated at low power for 2 h, followed by the addition of CA and acetone with another 2 h low-power sonication step. Sheath dispersions of TiO_2 were made at 3 wt % in 85:15 acetic acid/water and sonicated for 2 h. Dispersions with titania for surface loading of electrospun cellulose fibers were made at 2 wt % in water and sonicated 2 h prior to use. Aqueous Keyacid Blue solutions were made at a concentration of 0.1 wt % and aqueous sulforhodamine solutions were made at a concentration of 0.01 wt %. For X-ray diffraction (XRD) experiments, samples of titania were dispersed in water or 85:15 acetic acid/water as described above, followed by solvent evaporation at 125 °C.

Electrospinning. The electrospinning apparatus (Figure 1) used a variable high-voltage power supply (Glassman High Voltage). Solutions were pumped through an 18 gauge blunt needle for conventional electrospinning at a flow rate of 0.5−0.8 mL/h using a syringe pump (Stoelting Co.). For coaxial electrospinning with a concentric nozzle (Nisco Engineering) solutions were pumped at a core flow rate of 0.5−0.8 mL/h and a sheath flow rate of 0.05−0.3 mL/ or 0.2−0.4 mL/h for TiO_2 and TiO_2/CA solutions/dispersions, respectively. When using a dispersion of titania as the sheath solution, it is important to note that the flow rate needs to be carefully monitored as electrospraying of

titania occurs easily at higher flow rates. A positive voltage of 25 kV was applied between the spinneret and an aluminum collecting ground electrode separated by a distance of 11 cm. All electrospinning experiments were performed at room temperature.

Deacetylation of CA. CA fiber mats were deacetylated in 0.5 N KOH in ethanol for 30 min at room temperature. After 30 min, the fiber mats were placed in 0.5 N aqueous HCl, followed by an excess of 0.5 N aqueous KOH. The fiber mats were back neutralized by 0.5 N aqueous HCl.

TiO_2 Loading. The TiO_2 nanoparticle surface loading treatment was adapted from Meilert et al. (9) Cellulose fiber mats were placed in 40 mL of aqueous 2 wt % TiO_2 dispersion for one hour at 75 °C. The loaded TiO_2−cellulose fiber mats were then dried at 100 °C for 30 min, followed by sonication in water for 5 min to remove any unbound titania.

Sample Staining. Samples were stained with the abovementioned staining solutions at a volume of 50 μL. For the experiments described in Figure 8, the volume of red wine was doubled after each subsequent staining. For quantitative analysis experiments, electrospun fiber mats were mounted in a UV−vis spectrometer and stained with the Keyacid Blue solution. A white light source was used to illuminate the sample at 1 h intervals, after which a spectrum was recorded in absorption mode by measuring the absorption peak of Keyacid Blue at 628 nm.

Sample Washing. Samples were placed in a laundry detergent (3 wt %) solution under stirring for 1 h, followed by 30 min of stirring in water. Samples were then dried in air at room temperature.

Titanium Assay. The titanium (Ti) assay is adapted from Sedaira et al. (32) Various fiber samples (∼10 mg) were dissolved in one mL of 50% (w/v) ammonium sulfate in concentrated sulfuric acid at elevated temperature. One-hundred microliters of the fiber solution was then added to 20 mL of 0.3125% (w/v) 5-chlorosalicylic acid, 0.125 M $NaClO_4$ in 50:50 water/ethanol, adjusted to pH 3 ($\pm$0.1) with concentrated ammonium hydroxide, and diluted to 25 mL with water. Ti-containing samples turned yellow, indicative of the formation of a Ti/5-chlorosalicylic acid complex. The quantification of Ti was performed by measuring the absorption of the solution at 355 nm. A standard solution of Ti was made by dissolving titania nanoparticles in 50% (w/v) ammonium sulfate in concentrated sulfuric acid to a final concentration of 4 mg/mL at elevated temperature under reflux. The standard was added at varying volumes to the 5-chlorosalicylic acid solution in a similar fashion as described above in order to obtain a calibration curve.

Characterization. Fiber morphology was studied using a FEI/ Phillips XL30 field-emission environmental scanning electron microscope (FE-ESEM). The deacetylation process was confirmed with infrared (IR) spectroscopy using a Nicolet Nexus 870 FTIR spectrometer from Thermo Electron Corporation in adsorption mode. A halogen light source was used at a power density of ∼13 and ∼27 mW/cm^2 for stain discoloration/ decomposition experiments and UV−vis characterization experiments, respectively. UV−vis experiments were performed on a Perkin-Elmer Lambda 900 UV/vis/NIR spectrometer. The cross sections of photocatalytic electrospun fiber mats were analyzed using a JEOL 1230 Transmission Electron Microscope (TEM) operating at 80 kV. XRD patterns of titania samples were collected using a X'Pert Pro MPD X-ray diffractometer from PANalytical using Cu Kα_1 radiation.

RESULTS AND DISCUSSION

The deacetylation of electrospun CA fibers is an established method to obtain cellulose nanofibers (33−35). The reaction from CA to cellulose shown in Scheme 1 was confirmed for the electrospun fibers by IR spectroscopy. The

Scheme 1. Reaction of Cellulose Acetate with 0.5 N KOH in EtOH
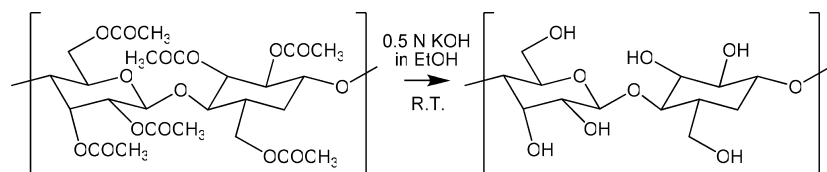
spectrum for CA (see Figure S1, black line, in the Supporting Information) contains the characteristic IR peaks associated with the acetyl group at 1745 cm^{-1} ($\nu_{C=O}$) and 1375 cm^{-1} (ν_{C-CH_3}). After 30 min of deacetylation, these peaks are absent from the IR spectrum (see Figure S1, red line, in the Supporting Information). Along with the significant increase in intensity for the C—OH peak at ~3500 cm^{-1}, this shows that the deacetylation process was successful and cellulose is obtained (34).

FE-SEM images of CA fibers and cellulose fibers are shown in Figure S2a and S2b (Supporting Information), respectively. The CA fibers have diameters that range from 100−600 nm, with the diameter of the majority of fibers at ~250 nm. At the surface, the cellulose fibers appear to have been changed very little by deacetylation. The cellulose fibers have a similar diameter range, with the majority at ~200 nm, slightly smaller than the native CA fibers. During deacetylation, acetyl groups are replaced by hydroxyl groups, changing from ~60% hydroxyl content of CA from manufacturer to nearly 100% hydroxyl content (see Figure S1 in the Supporting Information). This greatly increases the likelihood of hydrogen bonding in the fiber structure. Hydrogen bonding is known to play a crucial role in the structure of cellulose (36), and is the main reason for its low solubility in most solvents systems. The increase in secondary bonding within the structure and crystallographic differences between hydroxylated and acetylated cellulose (37, 38) are likely causes for the change in fiber diameter and morphology.

The morphology of cellulose—titania electrospun fibers using a coaxial nozzle was studied using FE-SEM. Selected examples indicative of important features are illustrated in the photomicrographs of Figure 2. Fibers electrospun with a blended TiO$_2$/CA sheath solution are shown in Figure 2a before deacetylation and in Figure 2b after deacetylation. Morphological differences between fibers created from conventional and coaxial nozzle configurations (Figure S1 vs Figure 2a) are clearly apparent. Asymmetrical and concave-like beads are formed and the fiber diameters are mostly around ~200 nm, with no fibers of diameters higher than ~300 nm being observed. The overall fiber thinning can be attributed to bead formation as the beads consume more polymer, reducing the amount available for fiber formation. This bead formation is not observed with conventionally electrospun CA nanofibers. Beads could be attributed to CA—TiO$_2$ clustering in solution as the titania binds to the CA. TiO$_2$ nanoparticles in clusters of varying sizes are observed adhering to fibers and within the beaded sections. Upon deacetylation, seminal morphological changes occur: beaded regions disappear, the average fiber diameter increases, and

titania coverage appears more widespread. A migration of nanoparticles during deacetylation could contribute to this effect because the TiO$_2$ nanoparticles would bind to the deacetylating solvent as well, which would allow for their diffusion through the deacetylating medium. Another possible explanation could be polymer chain rearrangement during deacetylation leading to the uncovering of previously embedded nanoparticles.

Fibers electrospun with a dispersion of TiO$_2$ as a sheath solution are shown Figure 2d (before deacetylation) and Figure 2e (after deacetylation). Unlike the previous case, fiber diameter and morphologies remain relatively unchanged upon deacetylation. Prior to deacetylation, titania appears mostly in aggregated clusters along the fibers, while the size and number of aggregates decrease after deacetylation. As for the case of TiO$_2$/CA sheath fibers, this could be attributed to nanoparticles migration in the deacetylating medium. Cellulose nanofibers surface-loaded with TiO$_2$ are shown in images g and h in Figure 2. Fiber diameter and morphology are comparable to cellulose (core)—TiO$_2$ (sheath) fibers, but the titania distribution varies greatly across the fiber mat. It is worth noting that the hydroxyl functionality in the cellulose fibers does not bind titania as well as carboxylic acid modified cellulose, which more uniformly binds TiO$_2$. As such, the latter is often used because of its advantageous titania binding ability (9, 11, 39). High-magnification SEM micrographs are shown in images c, f, and i in Figure 2 to better display the titania nanoparticle
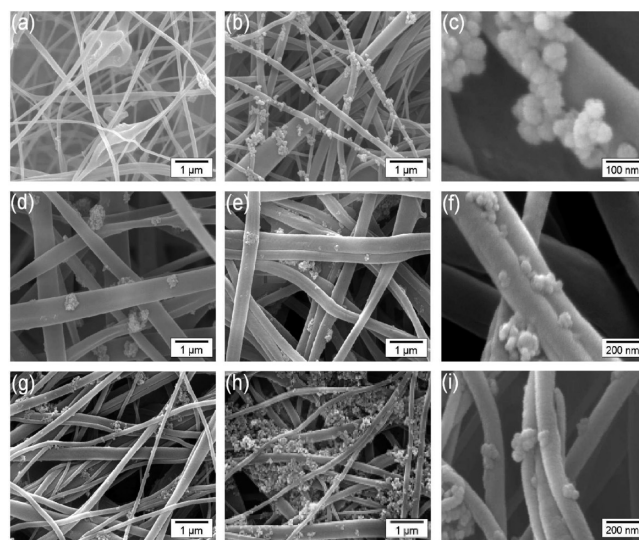

FIGURE 2. SEM microphotographs of TiO$_2$-containing nanofibers formed by coaxial electrospinning. CA (core)—TiO$_2$/CA (sheath): (a) as-spun; (b, c) post-deacetylation cellulose.CA (core)—TiO$_2$ (sheath): (d) as-spun; (e, f) post-deacetylation cellulose; (g−i) post-deacetylated cellulose fibers surface loaded with TiO$_2$.
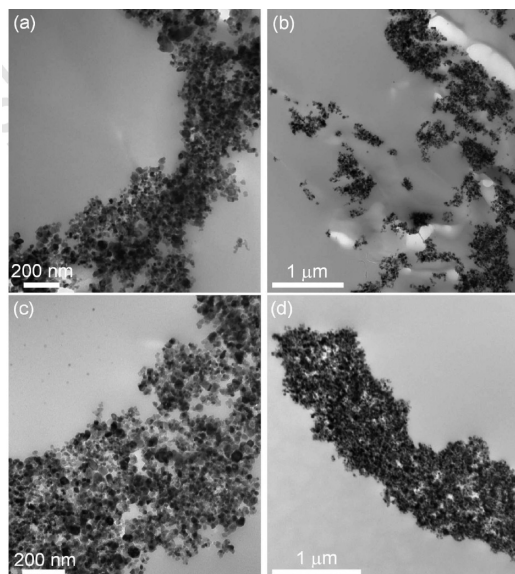
FIGURE 3. (a, b) TEM cross-section microphotographs of cellulose (core)−TiO$_2$ (sheath) fiber mats and (c, d) cellulose fibers surface-loaded with TiO$_2$.
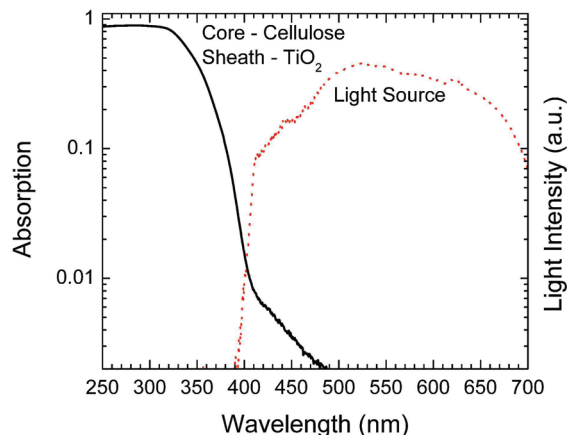

FIGURE 4. Optical spectra relevant to the self-cleaning process: TiO$_2$ nanoparticle absorption and halogen lamp emission.
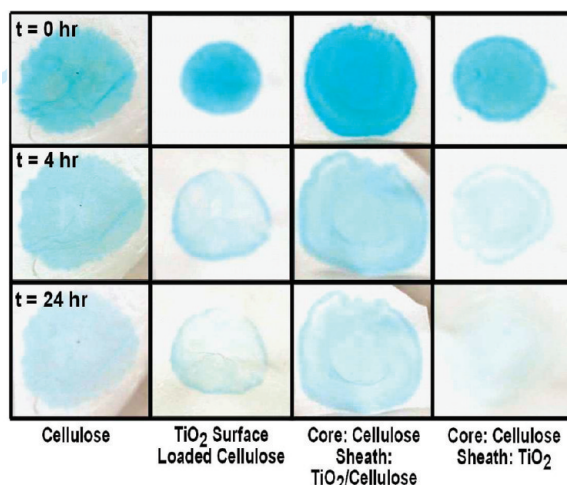

FIGURE 5. Photographs showing the discoloration of Keyacid Blue (0.1 wt %) stain in electrospun nonwoven mats exposed to halogen light (∼13 mW/cm^2) over a 24 h period: (a) cellulose nanofibers; (b) TiO$_2$ surface-loaded cellulose nanofibers; (c) cellulose (core)−TiO$_2$/cellulose (sheath) nanofibers; (d) cellulose (core)−TiO$_2$ (sheath) nanofibers.

clusters formed on cellulose fibers with various techniques. TEM cross sections are shown in Figure 3 for the fibers made by coaxial electrospinning and surface loading techniques. Because of the similar elemental composition of the epoxy used for casting and the cellulose nanofibers, contrast between the two materials is very low. In general, clusters of titania are seen throughout the cross-section of the fiber mats for both samples. At higher magnifications, the amount, distribution, and density of titania appear similar for samples made by coaxial electrospinning (Figure 3a) and surface loading (Figure 3c) methods. However, at lower magnification, it is clearly seen that the fibers made by coaxial electrospinning have a better titania distribution in the cross section compared to the more aggregated titania seen in samples made by surface loading (Figure 3b,d).

The photodegradation properties of the electrospun fibers were initially examined by testing the decomposition of a blue dye solution under halogen lamp irradiation. Halogen lighting is used because it better resembles indoor lighting conditions and represents the lower level of achievable photocatalytic activity. The halogen lamp emission spectrum is shown in Figure 4 along with the absorption spectrum of TiO$_2$ nanoparticles. The halogen lamp emits a very low number of photons in the UV range compared to visible range photons. As expected, the absorption of the TiO$_2$ measured from the electrospun cellulose fibers is mainly in the UV region, with a small amount extending into the visible range. The photocatalytic properties of titania allows for the small amount of near band gap light to be effectively used in molecular decomposition.

Figure 5 contains photographs illustrating the decomposition over a period of 24 h of Keyacid Blue dye solutions by plain cellulose nanofibers, TiO$_2$ surface loaded cellulose nanofibers, cellulose (core)−TiO$_2$/cellulose blend (sheath) nanofibers, and cellulose (core)−TiO$_2$ (sheath) nanofibers under halogen illumination at a power density of ∼13 mW/

cm^2. The cellulose nanofiber mat shows a slow discoloration with time and is used for reference. Titania surface loaded fibers do show photocatalytic activity. However, this type of fiber mat does not show full discoloration over the entire stained area. Fibers made using the coaxial nozzle with a TiO$_2$/cellulose blended sheath show little degradation despite the appearance of nanoparticles on the exterior of the fibers (Figure 2b). It is conceivable that the titania is covered in a thin layer of cellulose since the nanoparticles were initially in a solution with a partially hydroxyl functionalized polymer. This would then impede free radical generation and slow the self-cleaning process. Cellulose (core)−TiO$_2$ (sheath) fibers display the best self-cleaning characteristics as the blue dye solution is almost completely eliminated throughout the entire stain region after 24 h. For comparison, a mat of unreacted CA (core)−TiO$_2$ (sheath) fibers was stained using 0.1 wt % blue dye solution (Figure 6). Although the amount of dye is not fully degraded over the 24 h period, the fibers do exhibit significant photocatalytic activity. The intense initial dye color is due to the lower wettability of the CA
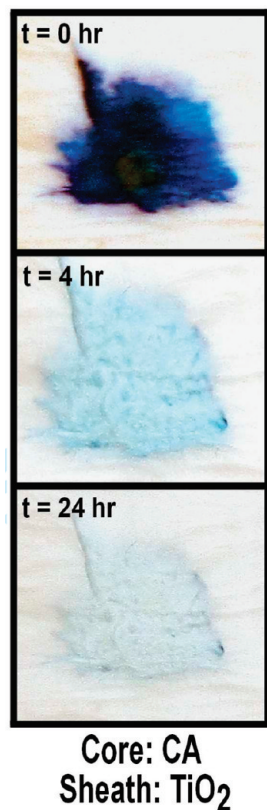
ARTICLE

FIGURE 6. Photographs showing the discoloration of Keyacid Blue (0.1 wt %) stain in coaxial electrospun non woven mats of CA (core)−TiO$_2$ (sheath) fibers exposed to halogen light (~13 mW/cm^2) over a 24 h period.

fibers. This shows that the catalytic properties of titania are largely unaffected by the deacetylation process.

Optical absorption of the fiber mats as a function of time is used to provide a quantitative evaluation of the decrease in Keyacid Blue dye concentration due the self-cleaning activity of various nanofibers. The results are shown in Figure 7. In these experiments, the concentration is normalized to the value at time equal to zero and the illuminator power density was ~27 mW/cm^2. It is assumed that to a first-order approximation the dye absorption in the fiber is linearly proportional to its concentration. The plain cellulose fibers show a nearly linear reduction in the dye absorption with time. After ten hours of halogen lamp exposure the fiber mat has reduced its dye concentration by ~30%, corresponding to a dye decomposition rate of 6.7×10^{-6} mM/min. All of the TiO$_2$-containing nanofibers exhibited a two-mode discoloration pattern, consisting of a rapid initial decay for the first one to two hours followed by a more slowly time-varying component. As observed qualitatively in the photographs of Figure 5, nanofibers with a blended TiO$_2$/cellulose sheath phase show slightly stronger chemical degradation than the pure cellulose nanofibers, reaching a 50% concentration after ten hours with an exponential decomposition rate constant of 4.5×10^{-6} mM/min. The cellulose (core)−TiO$_2$ (sheath) nanofibers decompose the dye molecules more quickly than the blended sheath nanofibers reaching a rate constant of 1.8×10^{-5} mM/min. In this case, the photocatalytic process is able to reach 100% dye de-
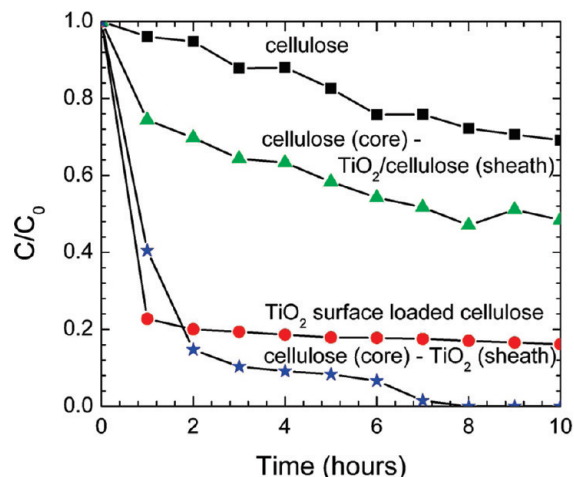

FIGURE 7. Concentration of Keyacid Blue (0.1 wt %) in electrospun nonwoven mats exposed to halogen light (~27 mW/cm^2) as a function of time: cellulose nanofibers (black squares), cellulose (core)−TiO$_2$/cellulose (sheath) nanofibers (green triangles), TiO$_2$ surface-loaded cellulose nanofibers (red circles), cellulose (core)−TiO$_2$ (sheath) nanofibers (blue stars).

composition (in ~7 h). The surface loaded nanofibers exhibit a quick degradation to ~20% of the initial dye concentration in less than 1 h, followed by a very slow concentration decay for the remainder of the exposure time (~9 h). The equivalent exponential decay rate constant of 6.1×10^{-5} mM/min is the fastest in the initial time regime. However, unlike the coaxial fibers the surface loaded photocatalytic process only reaches a maximum of 80% dye decomposition. The chemical decomposition characteristics of the coaxial electrospun derived and surface-loaded fiber mats are consistent with the amount of TiO$_2$ in each mat and with the method of its incorporation. The surface loaded mat is likely to have a non uniform TiO$_2$ concentration with the highest value near the top surface of the mat. This would result in faster initial decay, but because of the lower total amount of titania the ultimate decomposition will not be as complete as for the fiber mat made using coaxial electrospinning.

Initially, the surface density of dye molecules on the surface of the fiber mats for each sample is $\sim 3.8 \times 10^{15}$ dye molecules/cm^2, although the total flux of photons on the surface is $\sim 1.9 \times 10^{21}$ photons/cm^2 for the complete decomposition of the dye in the cellulose (core)−TiO$_2$ (sheath) example. This corresponds to one dye molecule decomposing for every 5×10^5 photons. Clearly, the vast majority of photons are not utilized in the decomposition process because of the very low absorption in the visible range. However, the coaxial electrospinning method allows for a larger quantity of TiO$_2$ to be embedded into the nonwoven mat, leading to the full decomposition of the dye molecules in 7 to 8 h. It is anticipated that using N- and/or F-doped TiO$_2$, which has a lower bandgap (40), will reduce the total decomposition from hours to minutes.

Ti assay and XRD experiments were performed in order to better understand the photocatalytic properties of the fiber mats made by coaxial electrospinning and by surface loading techniques. The Ti assay is used to quantify the amount of titania present in the fiber mats. From Figure S3
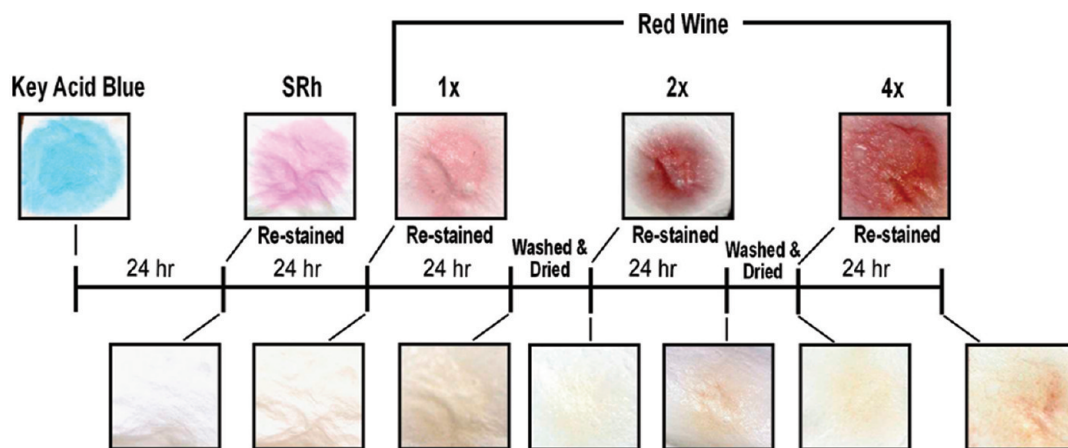
FIGURE 8. Photographs of nonwoven mat formed by cellulose (core)–TiO$_2$ (sheath) fibers sequentially stained with dye solution (Keyacid Blue and sulforhodamine) and wine, halogen irradiated, and washed and dried. From left to right: Keyacid Blue (0.1 wt %) solution; restained with sulforhodamine (0.01 wt %) solution; restained with red wine; washed, dried, and restained with twice the amount of red wine; then washed, dried, and completely saturated with four times the amount of red wine.

(see the Supporting Information), the concentration of Ti in the surface loaded fibers in solution is 0.04 ± 0.01 mM, whereas the solution from the fiber mats made by coaxial electrospinning is 0.03 ± 0.01 mM. This corresponds to a titania/fiber mat percentage of 7.3 and 4.5 ± 1.7 %, respectively, indicating that the amount of titania in the surface loaded electrospun fibers mats is slightly larger compared to the fibers made by coaxial electrospinning. To determine any crystallographic differences between the titania in the surface-loaded and coaxial electrospun fiber mats, we made titania nanoparticle dispersions in a similar fashion as used for coaxial electrospinning (85 % acetic acid dispersion) and for surface loading (aqueous dispersion), followed by the removal of the solvent. In the perspective of the whole diffraction pattern, it appears the patterns are identical (see Figure S4 in the Supporting Information), exhibiting all the characteristic peaks for P-25 titania. However, upon closer inspection (inset, Figure S4 in the Supporting Information) it becomes clear that the crystallite size for the nanoparticles treated in water (surface-loaded fibers) is larger than those treated in 85 % acetic acid (coaxial electrospun fibers). Using the Scherrer equation (41), it was estimated that the crystallite size for water and 85 % acetic acid treated samples are 17.4 ± 0.9 nm, and 14.8 ± 0.5 nm respectively. A decrease in crystallite size is known to increase photocatalytic activity (42), while differences in crystallite sizes have been observed in titania films cast in different solvents following sonication (43). Despite the slightly larger amount of titania measured in the photocatalytic fiber mats made by surface loading techniques, the fibers made by coaxial electrospinning exhibit a more complete photocatalytic degradation of the analytes tested. This is probably due to the higher uniformity of the titania along the fibers and within the fiber mats compared to surface loading methods (Figure 2e vs Figure 2g and Figure 2h; Figure 3b vs Figure 3d) and to a lesser extent to the smaller crystallite size titania present in the coaxial electrospun fibers.

To study both the durability and safety of the photocatalytic cellulose nanofibers, we performed longevity tests to determine the multiple-use performance and adherence of

the titania to the nanofibers, as the safety of nanoscale TiO$_2$ has come into question (44, 45). Photographs of the fiber mat at different stages of the process are shown in Figure 8. Using the same lighting conditions as the experiments described in Figure 5, the electrospun fibers made by coaxial electrospinning with a titania sheath were first stained with the Keyacid Blue dye solution, and then exposed to halogen irradiation to obtain self-cleaning through photodegradation. After 24 h, the same sample was restained with a sulforhodamine dye solution. Within the next 24 h, the stain is again nearly 100 % removed from the sample by photodegradation. This sample was stained a third time with red wine, again becoming discolored within 24 h. The sample was next washed (using the procedure described in the experimental section), after which the sample was completely white. An increased amount (2×) of red wine was used for the fourth staining of the sample, and a similar discoloration is observed once again. Following a second washing step, an even larger amount of red wine was used for the fifth and final staining (four times the initial red wine staining), fully saturating the sample. The final discoloration effect is not as pronounced as in the previous trials, yet there is still an observable cleaning effect, even after multiple staining and washing processes. SEM photographs of these fibers after the initial staining only and after one staining, washing, and drying cycle are shown in images a and b in Figure 9. These images show that the morphology of the cellulose fibers is unchanged and titania is still bound throughout the staining and washing processes. For reference, an SEM photograph of cellulose fibers (without TiO$_2$) after staining and exposure to halogen light is shown in Figure 9c.

CONCLUSIONS

Photocatalytic self-cleaning textile nanofibers have been created using coaxial electrospinning. Self-cleaning activity is obtained in light typical of an indoor working environment. It was found that fibers created by coaxial electrospinning outperform those made by simple loading procedures and have the added benefit of requiring less post-electrospinning modification. It is worth noting that
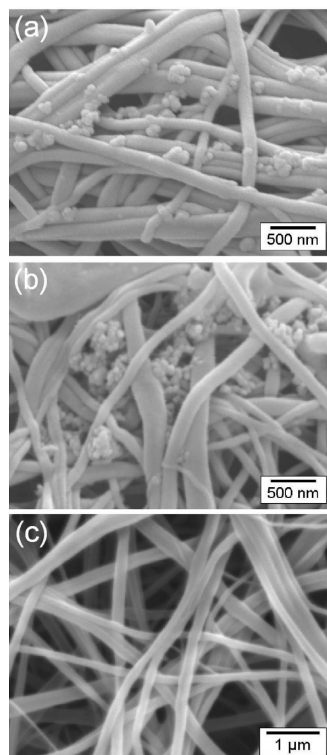
FIGURE 9. SEM microphotographs of (a) cellulose (core)−TiO₂ (sheath) fibers after being stained with a 0.1 wt % Keyacid Blue solution and irradiated with ∼13 mW/cm² halogen lighting for 24 h; (b) cellulose (core)−TiO₂ (sheath) fibers after being stained with a 0.1 wt % Keyacid Blue solution, irradiated with ∼13 mW/cm² halogen lighting for 24 h, and washed and dried as described in the experimental section; and (c) cellulose fibers after being stained with a 0.1 wt % Keyacid Blue solution and irradiated with ∼13 mW/cm² halogen lighting for 24 h.

this study represents the lowest possible photocatalytic activity using this method. A more efficient photocatalyst (nitrogen or fluorine doped TiO₂, and noble metal doped/ bound TiO₂ for example) could be used to further accelerate the self-cleaning performance. Different chemical functionalities can be employed to improve the adherence of the titania to the polymer, while testing in UV light would also increase the photocatalytic behavior seen in these experiments. In light of these considerations, it is concluded that the photocatalytic self-cleaning textile fibers fabricated by coaxial electrospinning are comparable to nonelectrospun photocatalytic self-cleaning textile fibers seen in the literature that use better photocatalytic materials and sub-band gap wavelength light sources. This illustrates the important role played by the high surface to volume ratio of the material fabricated by coaxial electrospinning. The results of this study clearly show the versatility of coaxial electrospinning in general and more specifically indicate the promise of using this method for self-cleaning textiles applications.

Supporting Information Available: IR absorption spectrum and SEM microphotographs of CA and deacetylated cellulose fibers; 355 nm absorption of Ti from Ti/5-chlorosalicylic acid as a function of Ti in solution for various fibers; XRD patterns from P-25 titania cast from H₂O and acetic acid/H₂O solutions (PDF). This material is available free of charge via the Internet at http://pubs.acs.org.

REFERENCES AND NOTES

(1) Molinari, R.; Mungari, M.; Drioli, E.; Di Paola, A.; Loddo, V.; Palmisano, L.; Schiavello, M. *Catal. Today* **2000**, *55*, 71−78.
(2) Vorontsov, A. V.; Chen, Y.-C.; Smirniotis, P. G. *J. Haz. Mater.* **2004**, *B113*, 89−95.
(3) Štengl, V.; Maøiková, M.; Bakardjieva, S.; Šubrt, J.; Opluštil, F.; Olšanska, M. *J. Chem. Technol. Biotechnol.* **2005**, *18*, 754−758.
(4) Uddin, M. J.; Cesano, F.; Scarano, D.; Bonino, F.; Agostini, G.; Spoto, G.; Bordiga, S.; Zecchina, A. *J Photochem. Photobiol., A: Chem.* **2008**, *199*, 64−72.
(5) Zhao, X.; Zhao, Q.; Yu, J.; Liu, B. *J. Non-Cryst. Solids* **2008**, *354*, 1424−1430.
(6) Madaeni, S. S.; Ghaemi, N. *J. Membr. Sci.* **2007**, *303*, 221−233.
(7) Hoffmann, M. R.; Martin, S. T.; Choi, W.; Behnemann, D. W. *Chem. Rev.* **1995**, *95*, 69−96.
(8) Abidi, N.; Cabrales, L.; Hequet, E. *ACS Appl. Mater. Interfaces* **2009**, *1*, 2141−2146.
(9) Meilert, K. T.; Laub, D.; Kiwi, J. *J. Mol. Catal., A: Chem.* **2005**, *237*, 101−108.
(10) Textor, T.; Schröter, F.; Schollmeyer, E. *Macromol. Symp.* **2007**, *254*, 196−202.
(11) Daoud, W. A.; Leung, S. K.; Tung, W. S.; Xin, J. H.; Cheuk, K.; Qi, K. *Chem. Mater.* **2008**, *20*, 1242−1244.
(12) Li, D.; Xia, Y. *Adv. Mater.* **2004**, *16*, 1151−1170.
(13) Powell, H. M.; Boyce, S. T. *J. Biomed. Res., Part A* **2007**, *84A*, 1078−1086.
(14) Kenawy, E.-R.; Bowlin, G. L.; Mansfield, K.; Layman, J.; Simpson, D. G.; Sanders, E. H.; Wnek, G. E. *J. Controlled Release* **2002**, *81*, 57−64.
(15) Liu, H.; Kameoka, J.; Czaplewski, D. A.; Craighead, H. G. *Nano Lett.* **2004**, *4*, 671−675.
(16) Ma, M.; Gupta, M.; Li, Z.; Zhai, L.; Gleason, K. K.; Cohen, R. E.; Rubner, M. F.; Rutledge, G. C. *Adv. Mater.* **2007**, *19*, 255−259.
(17) Han, D.; Steckl, A. J. *Langmuir* **2009**, *25* (16), 9454−9462.
(18) Li, D.; Xia, Y. *Nano Lett.* **2003**, *3*, 555−560.
(19) Lee, J. A.; Krogman, K. C.; Ma, M.; Hill, R. M.; Hammond, P. T.; Rutledge, G. C. *Adv. Mater.* **2009**, *21*, 1252−1256.
(20) Yu, J. H.; Fridrikh, S. V.; Rutledge, G. C. *Adv. Mater.* **2004**, *16*, 1562−1566.
(21) Li, D.; Xia, Y. *Nano Lett.* **2004**, *4*, 933−938.
(22) Wang, M.; Jing, N.; Su, C. B.; Kameoka, J.; Chou, C.-K.; Hung, M.-C.; Chang, K.-A. *Appl. Phys. Lett.* **2006**, *88*, 033106.
(23) Han, X.-J.; Huang, Z.-M.; He, C.-C.; Liu, L.; Han, X.-J.; Wu, Q.-S. *Polym. Compos.* **2006**, *27*, 381−387.
(24) Heinze, T.; Liebert, T. *Prog. Polym. Sci.* **2001**, *26*, 1689−1762.
(25) Hurum, D. C.; Agrios, A. G.; Gray, K. A.; Rajh, T.; Thurnauer, M. C. *J. Phys. Chem. B* **2003**, *107*, 4545−4549.
(26) Hurum, D. C.; Gray, K. A.; Rajh, T.; Thurnauer, M. C. *J. Phys. Chem. B* **2005**, *109*, 977−980.
(27) Linkous, C. A.; Carter, G. J.; Locuson, D. B.; Ouellette, A. J.; Slattery, D. K.; Smitha, L. A. *Environ. Sci. Technol.* **2000**, *34*, 4754−4758.
(28) Yu, J. C.; Yu, J.; Zhao, J. *Appl. Catal., B: Environ.* **2002**, *36*, 31−43.
(29) Cao, Y.; Yang, W.; Chen, Y.; Du, H.; Yue, P. *Appl. Sur. Sci.* **2004**, *236*, 223−230.
(30) Nagaveni, K.; Sivalingam, G.; Hegde, M. S.; Madras, G. *Appl. Catal., B: Environ.* **2004**, *48*, 83−93.
(31) Han, S.-O.; Youk, J.-H.; Min, K.-D.; Kang, Y.-O.; Park, W.-H. *Mater. Lett.* **2008**, *62*, 759−762.
(32) Sedaira, H.; Idriss, K. A.; Shafei Abdel-Aziz, M. *Analyst* **1996**, *121*, 1079−1084.
(33) Liu, H.; Hsieh, Y.-L. *J. Polym. Sci., Part B: Polym. Phys.* **2002**, *40*, 2119−2129.
(34) Son, W. K.; Youk, J. H.; Lee, T. S.; Park, W. H. *J. Polym. Sci., Part B: Polym. Phys.* **2004**, *42*, 5−11.

(35) Ma, Z.; Kotaki, M.; Ramakrishna, S. *J. Membr. Sci.* **2005**, *265*, 115–123.

(36) Zhao, H.; Kwak, J. H.; Wang, Y.; Franz, J. A.; White, J. M.; Holladay, J. E. *Carbohydr. Polym.* **2007**, *67*, 97–103.

(37) Nishiyama, Y.; Langan, P.; Chanzy, H. *J. Am. Chem. Soc.* **2002**, *124*, 9074–9082.

(38) Stipanovic, A. J.; Sarko, A. *Polymer* **1978**, *19*, 3–8.

(39) Yuranova, T.; Laub, D.; Kiwi, J. *Catal. Today* **2007**, *122*, 109–117.

(40) Pelaez, M.; de la Cruz, A. A.; Stathatos, E.; Falaras, P.; Dionysiou, D. D. *Catal. Today* **2009**, *144*, 19–25.

(41) Gao, L.; Li, Q.; Song, Z.; Wang, J. *Sens. Actuators, B* **2000**, *71*, 179.

(42) Anpo, M.; Shima, T.; Kodama, S.; Kubokawa, Y. *J. Phys. Chem.* **1987**, *91*, 4305.

(43) Uzunova-Bujnova, M.; Todorovska, R.; Milanova, M.; Kralchevska, R.; Todorovsky, D. *Appl. Sur. Sci.* **2009**, *256*, 830.

(44) Lu, N.; Zhu, Z.; Zhao, X.; Tao, R.; Yang, X.; Gao, Z. *Biochem. Biophys. Res. Commun.* **2008**, *370*, 675–680.

(45) Chen, H.-W.; Su, S.-F.; Chien, C.-T.; Lin, W.-H.; Yu, S.-L.; Chou, C.-C.; Chen, J. J. W.; Yang, P.-C. *Fed. Am. Soc. Exp. Biol. J.* **2006**, *20*, E1732–E1741.

AM1005089